$$\mathrm{NSE}_Q = 1 - \frac{\sum_{t=1}^{T}\left(Q_s^t - Q_o^t\right)^2}{\sum_{t=1}^{T}\left(Q_o^t - \bar{Q}_o\right)^2} \tag{8}$$

$$\mathrm{NSE}_{LogQ} = 1 - \frac{\sum_{t=1}^{T}\left(LogQ_s^t - LogQ_o^t\right)^2}{\sum_{t=1}^{T}\left(LogQ_o^t - \overline{LogQ}_o\right)^2} \tag{9}$$

where $Q_s^t$ and $Q_o^t$ represent the simulated and observed flow in daily time step, respectively. $\bar{Q}_o$ and $\overline{LogQ}_o$ are the average observed flow and the average logarithm of flow, respectively, over the calibration period. The output of the two-objective calibration is a Pareto front of multiple solutions, and the following Euclidean Distance (ED) formula (Eq. 10) is used to identify a single best model run (Hrachowitz and Clark, 2017).

$$\mathrm{ED} = \sqrt{\left(1 - NSE_Q\right)^2 + \left(1 - NSE_{LogQ}\right)^2} \tag{10}$$

The MOPSO algorithm was used to calibrate the two-objective hydrological model (Coello et al., 2004). Fig. 9 illustrates the step-by-step procedure of MOPSO and its interaction with the hydrological rainfall-runoff model. In MOPSO, the algorithm starts by creating a random population of $x_i$ particles (Fig. 9b), so that each particle has an n-dimensional set for $n$ calibration parameters. In this study, each particle is a 6-parameter set of snow and soil moisture storage calibration parameters $\{SWC, K, RRF, Z_1, T_F, T_M\}$(see Table 3 and Table 4), with upper and lower limits shown in Table 6. Each particle represents a set of calibration parameters used to run the hydrological model for the entire simulation period (2001–2014) on a daily time scale. Daily flow and logarithm flow are simulated by the hydrologic model, and they are imported to the optimization model for calculating the objective functions. The process is repeated for each particle in the current population. Finally, non-dominated particles in the population are saved and added to the Pareto set. If the stopping criterion of the optimization model is not reached, a new population of particles is generated by the optimization algorithm, and the entire procedure is repeated. Finally, the best parameters set of Pareto fronts with the minimum ED is selected for the hydrological rainfall-runoff model. More details about MOPSO and its parameters are presented in (Coello et al., 2004; Dehghanipour

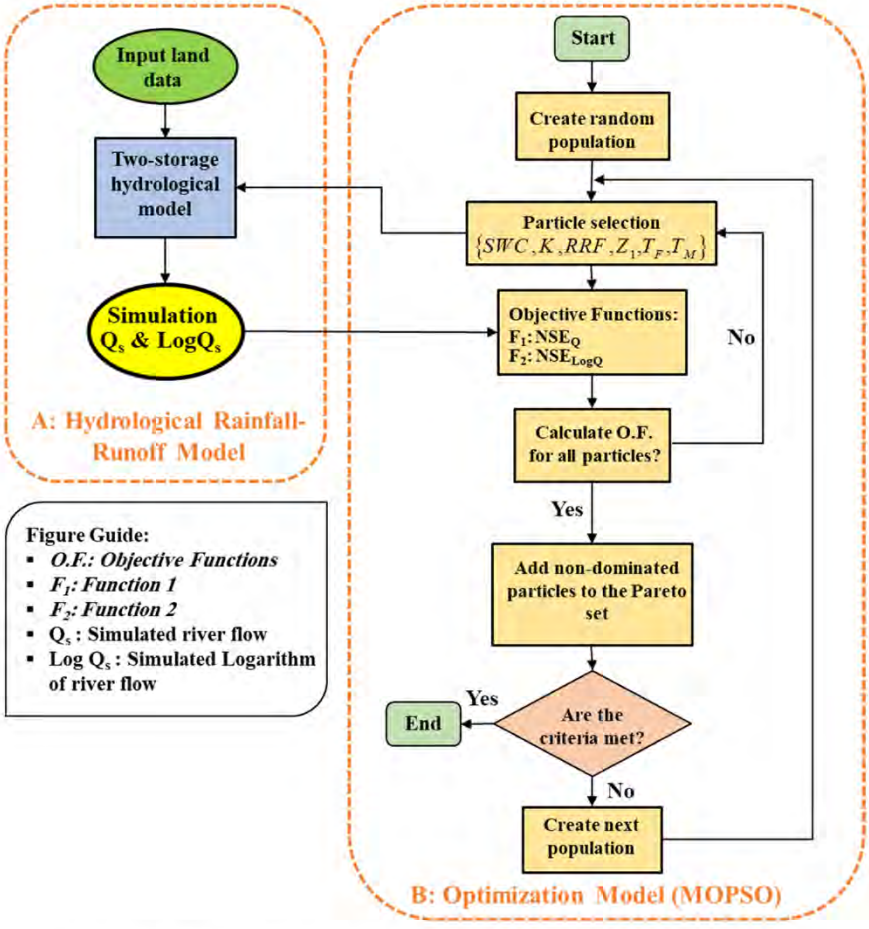


**Fig. 9.** Outline of calibration of hydrological rainfall-runoff model using MOPSO.

**Table 6**
Calibration parameters and their threshold for Hydrological Rainfall-Runoff Model. These parameters are determined for each sub-basin (Fig. 1b).

| Parameter | SWC | RRF | K | $Z_1$ | $T_{Freezing}$ | $T_{Melting}$ |
|---|---|---|---|---|---|---|
| **Unit** | mm | No unit | mm/day | No unit | °C | °C |
| **Description** | Soil water capacity | Runoff resistance factor | Root zone conductivity | Initial Relative soil water content | Freezing point | Melting Point |
| **Min** | 50 | 0 | 0 | 5 | -2.5 | $T_{Freezing}$ Value |
| **Max** | 1500 | 20 | 300 | 45 | 2.5 | 10 |

et al., 2019).

The calibration period was considered for 11 years in a daily time step (A total of 4018 time steps) for the period 2003–2014. Moreover, the period of 1999–2003 (1826 time steps) was examined as a validation period.

## 4. Results

### 4.1. Weather forecast downscaling

#### 4.1.1. AI downscaling methods

For a better understanding of the functionality of the mentioned AI methods in downscaling weather forecasts, the efficiency of each method was examined separately. Table 7 summarizes the efficiency criteria of downscaled precipitation forecasts for Tekab and Saqez synoptic stations. The optimization results show that the hybrid approach has far better efficiency than SVR and GMDH for ECMWF and NCEP data. In this case, NSE values of the hybrid approach were twice those of the non-hybrid methods.

The results also show the better performance of the ECMWF monthly precipitation forecasts for both stations and on both test and train data. In all three optimization methods, the optimization results of ECMWF are much better than NCEP. One reason is their different approach in forecasting weather conditions. NCEP uses a hydrostatic model combined with approximate estimates of topography. ECMWF, on the other hand, uses a non-hydrostatic model and more precisely accounts for topographic effects on the weather forecast (Owens and Hewson, 2018; Saha et al., 2010). Therefore, ECMWF has better performance in mountainous areas (Sodoudi et al., 2010). Moreover, test data had higher NSE than train data as the (end of the) test data period benefits from ECMWF's new update to SEAS5 in 2017, which includes an upgraded resolution and many other features.

Table 8 shows that results of downscaling daily temperature at 2 m are similar for both NCEP and ECMWF forecasts. Downscaling temperature with the GMDH method is acceptable since the temperature is not a random phenomenon like precipitation, and there is no significant benefit in using a more complex hybrid method. The corresponding forecast time series in Fig. 10 show that the GMDH downscaling method is capable of reducing the difference between observed and raw forecast data.

#### 4.1.2. BBN downscaling method

The BBN precipitation forecast model was used to forecast monthly precipitation. For validating the trained network, Accuracy criteria, confusion matrix (Table 9), and ROC Curve (Fig. 11) were calculated for the child (output) node. These are BBN's probabilistic results for showing its efficiency (BayesFusion, 2017). The ROC Curve for forecasting precipitation at Saqez station is shown in Fig. 11. The corresponding confusion matrix and accuracy criterion of the station are presented in Table 9 and Table 10, respectively. The values of the area under the ROC curve (AUC) for all precipitation categories are shown in Table 10. The numbers on the main diameter of the confusion matrix are more significant than the other arrays, indicating that the trained BBN simulates the true positive and the false positive with reasonable accuracy for different categories. Moreover, the Accuracy and AUC values for different categories are close to 1, indicating the BBN's acceptable performance and accuracy.

#### 4.1.3. Comparison of BBN and hybrid AI downscaling methods

Fig. 12 shows the train and test results of precipitation downscaling methods and observed data, in which BBN method was better able to fit the diagram with observed data. Furthermore, the downscaled forecasts from the BBN and hybrid AI methods in 2020 and 2021 were compared with the observed precipitation data at Saqez station (Fig. 13 and Table 11). The probabilistic categorical

**Table 7**
Efficiency criteria of downscaled ECMWF and NCEP precipitation forecasts for a 1-month lead time.

| | | ECMWF | | | | | | NCEP | | | | | |
|---|---|---|---|---|---|---|---|---|---|---|---|---|---|
| | | SVR | | GMDH | | SVR-GMDH (Hybrid) | | SVR | | GMDH | | SVR-GMDH (Hybrid) | |
| | | NSE | RMSE | NSE | RMSE | NSE | RMSE | NSE | RMSE | NSE | RMSE | NSE | RMSE |
| **Tekab station** | Train data | 0.27 | 0.08 | 0.16 | 0.34 | 0.54 | 1.00 | 0.24 | 3.54 | 0.18 | 4.50 | 0.33 | 3.59 |
| | Test data | 0.34 | 4.44 | 0.27 | 6.04 | 0.61 | 3.54 | 0.27 | 1.52 | 0.18 | 0.08 | 0.39 | 1.44 |
| **Saqez station** | Train data | 0.22 | 2.44 | 0.24 | 2.79 | 0.53 | 1.90 | 0.16 | 6.25 | 0.11 | 6.37 | 0.37 | 6.38 |
| | Test data | 0.37 | 2.68 | 0.54 | 3.4 | 0.62 | 2.43 | 0.28 | 3.79 | 0.31 | 4.28 | 0.41 | 3.76 |

**Table 8**
Efficiency criteria of downscaled ECMWF and NCEP temperature forecasts for 6-month lead time.

| | | GMDH | | | |
|---|---|---|---|---|---|
| | | ECMWF | | NCEP | |
| | | NSE | RMSE | NSE | RMSE |
| **Tekab station** | Train data | 0.81 | 0.01 | 0.86 | 0.01 |
| | Test data | 0.86 | 0.09 | 0.84 | 0.01 |
| **Saqez station** | Train data | 0.76 | 0.04 | 0.83 | 0.01 |
| | Test data | 0.84 | 0.13 | 0.81 | 0.01 |

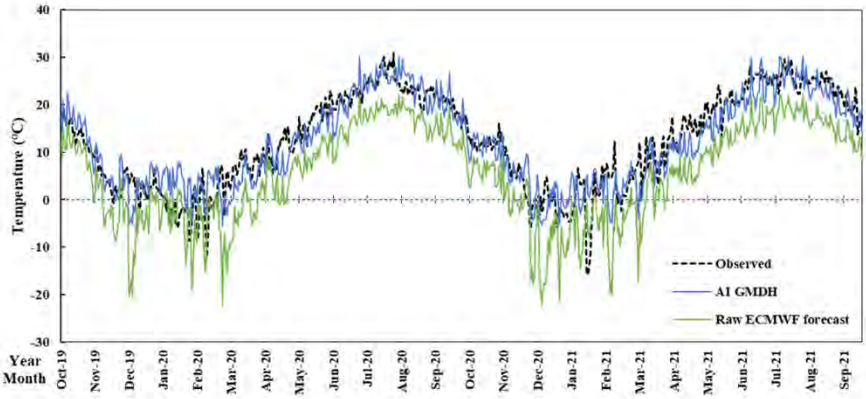


**Fig. 10.** Comparison of raw (ECMWF) and downscaled daily temperature forecasts at Saqez station using the GMDH downscaling method.

**Table 9**
Confusion matrix for downscaled precipitation at Saqez station.

| | | Simulated | | | | |
|---|---|---|---|---|---|---|
| | | S1 | S2 | S3 | S4 | S5 |
| **Observed** | S1 | 33 | 0 | 0 | 0 | 0 |
| | S2 | 7 | 25 | 1 | 0 | 0 |
| | S3 | 3 | 4 | 27 | 0 | 0 |
| | S4 | 0 | 1 | 2 | 29 | 1 |
| | S5 | 0 | 2 | 1 | 5 | 25 |

forecasts from the BBN model were converted into a single-value forecast by computing the average of each precipitation category weighted by the forecast probability of each category. Fig. 13 and Table 11 show the BBN has a better performance in downscaling precipitation, and it better captures the dynamics in the observed data.

A possible reason for the better performance may be due to the probabilistic nature of the BBN in better capturing the random nature of precipitation dynamics compared to the deterministic AI methods. As discussed earlier, the deterministic methods work better for temperature, which generally has greater predictability.

### *4.2. Hydrological model calibration*

In this study, a computer was used with a 2.8 GHz CPU and 16 GB of RAM. The running time of the hydrological rainfall-runoff model and optimization model took 35 s in the daily time step. About 30 s was dedicated to the running time of the hydrological model and about 5 s to call the results of runoff simulation, calculate the objective functions in the calibration process, and apply new calibration parameters to the hydrological model. Fig. 14 shows optimization results of the MOPSO algorithm after 7250 model runs for Saruq river sub-basin. It shows no significant trade-off between the two objective functions, and improving one objective function does not significantly affect the performance of the other objective function. This suggests that the rainfall-runoff model adequately captures both low flows (baseflow) and high flows.

However, many errors and uncertainties would occur in a single-objective calibration approach for estimating parameters. For instance, in Fig. 14, the three points A, B, and C correspond to maximum simulation accuracy of the logarithm of flow, the minimum ED, and maximum simulation accuracy of flow, respectively. Based on Fig. 14, if the one-objective calibration was applied to maximize $NSE_{logQ}$, the value would be 0.55 for $NSE_{LogQ}$ (corresponding to point A). This value is slightly higher than the value corresponding to the minimum ED in a two-objective calibration of 0.54 (point B); but the $NSE_Q$ in the single-objective calibration was 0.2 (point A),

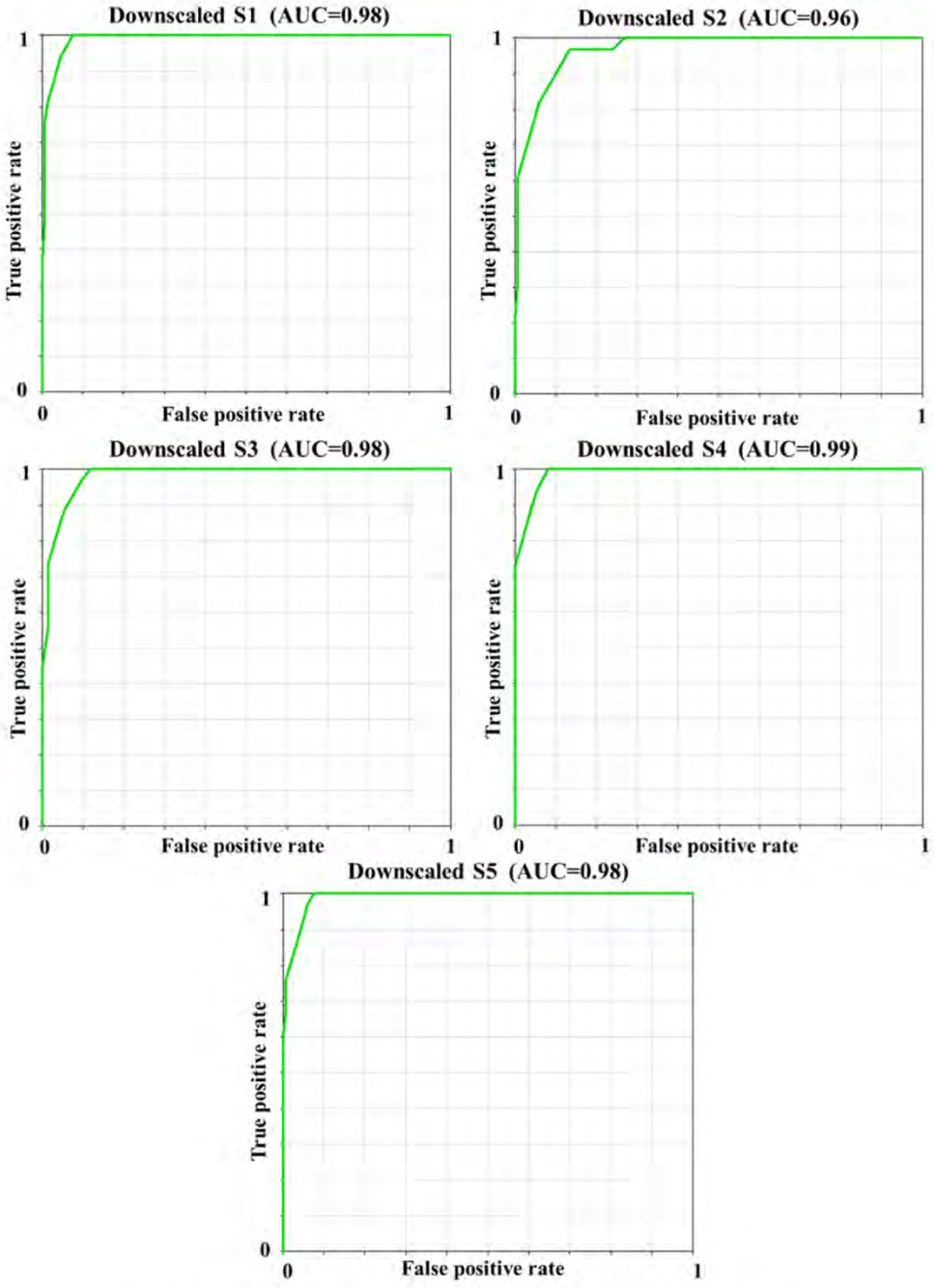


**Fig. 11.** ROC Curve of different categories for downscaled precipitation (Table 2).

**Table 10**
Accuracy and area under ROC curve for downscaled precipitation at Saqez station.

| | Area under receiver operating characteristic curve (AUC) | Accuracy |
|---|---|---|
| S1 | 0.98 | 0.84 |
| S2 | 0.96 | |
| S3 | 0.98 | |
| S4 | 0.99 | |
| S5 | 0.98 | |

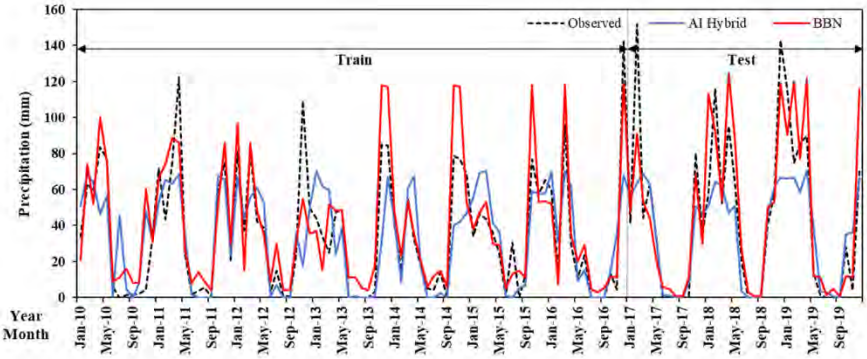


**Fig. 12.** Train and test results: Monthly time series of observed precipitation and 1-month forecasted precipitation by BBN and hybrid AI methods at Saqez station.

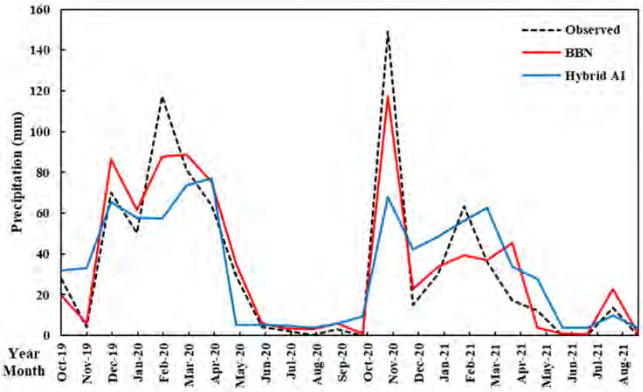


**Fig. 13.** Comparison of 1-month precipitation forecasts by the BBN and hybrid AI methods with observed precipitation in 2020 and 2021 at Saqez station.

**Table 11**
Efficiency of BBN and hybrid AI methods for 1-month precipitation forecasts in the years 2020 and 2021 at Saqez station.

| | BBN | Hybrid AI |
|---|---|---|
| **NSE** | 0.88 | 0.61 |
| **RMSE** | 13.24 | 24.54 |

which is very different from the value corresponding to the minimum ED in the two-objective calibration, which is equal to 0.55 (point B). Convergence of the MOPSO calibration was assessed by visual inspection of the Pareto front and the calibration was stopped when the Pareto front did not show significant changes between successive iterations.

Fig. 15 shows scatter diagrams of the objective functions versus the calibration parameters for the Saruq river sub-basin. When SWC increases, the two objective functions first increase and then decrease with an optimal value around 300 mm. The concentration of scatter points around the vertical axis in the plots for parameters K and $Z_1$ is evident for both objective functions, indicating that optimal values for these parameters are close to their lower limit (Table 6). $Z_1$ corresponds to the relative soil water content at the start of the simulation (1 October), when rainfall is low, and soils are likely dry. Likewise, the small value for parameter K reflects the mountainous nature of the region, with soils having low permeability. According to Fig. 15, values of the objective functions are highly sensitive to the parameters representing freezing and melting temperature, as would be expected in a region where runoff is affected by significant snow accumulation and snowmelt.

Optimal values of the calibration parameters in ZRR upstream, Saqez River, Saruq River, and Khoorkhooreh River sub-basins corresponding to Maximum $NSE_Q$, Maximum $NSE_{LogQ}$, and minimum ED are summarized in Table 12. The results of this Table show that the optimum freezing point ($T_F$) and melting point ($T_M$) for the snow storage of these sub-basins are close to the upper limit of these parameters in Table 6. By examining the region's data, we considered values up to 10 °C for melting parameter ($T_M$) since it may take until May (with average temperature of 10 °C) for snow to completely disappear. This shows the mountainous nature of the study area and snow's predominant role in the water balance equation, indicating the early freezing of precipitation in winter and the

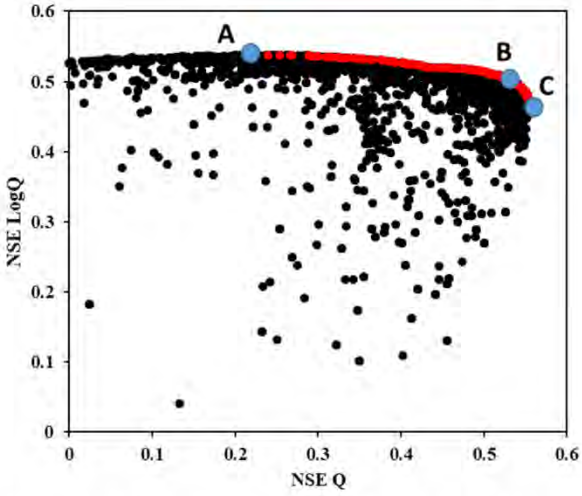


**Fig. 14.** Pareto plot for the multi-objective calibration after 7250 model simulations for Saruq river sub-basin with the MOPSO algorithm. Each point shows one simulation of the hydrological rainfall-runoff model, red points indicate the Pareto front, i.e. the set of non-dominated simulations.

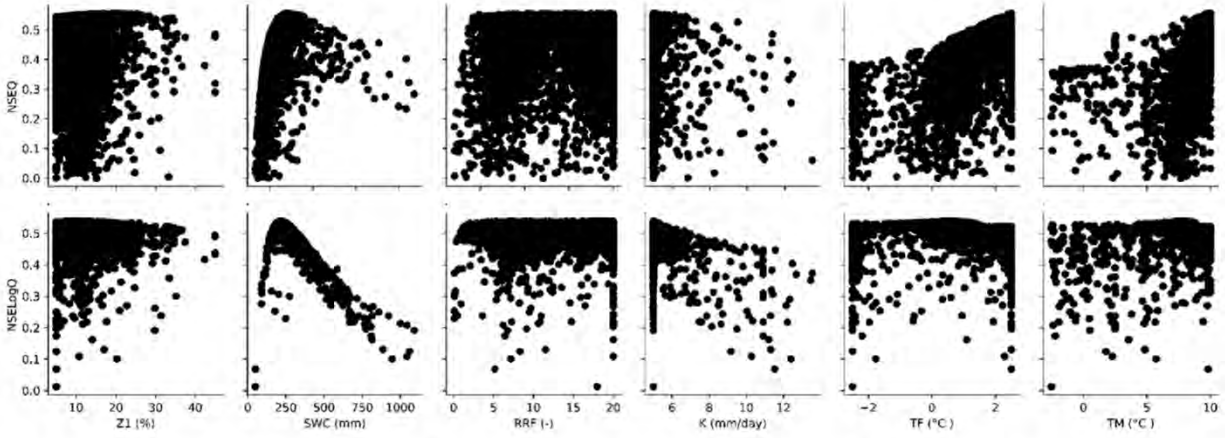


**Fig. 15.** Scatter plots of all calibration parameters and two objective functions for Saruq river sub-basin.

late melting of snow in spring. Furthermore, as discussed earlier, $Z_1$ and K are closer to their lower limits (Table 12).

Table 13 shows NSE values for simulating daily river runoff and logarithm of flow for each sub-basin during calibration and validation periods. Most NSE values in this table are above 0.5. Similar or lower NSE values (0.4–0.5) were obtained in previous simulation studies for this basin (Emami and Koch, 2019; Moriasi et al., 2007), with the critical caveat that those were based on monthly flows, whereas here we calculate the performance of daily flow simulations.

For instance, Fig. 16 shows simulated and observed time series of Saruq River flow. The NSE results of Table 13 and the comparison of simulated and observed flow in Fig. 16 show the model's acceptable performance in simulating wet and dry periods within the year as well as simulating drought and wet years.

Finally, precipitation and temperature outputs of the weather forecast downscaling model were used to force the hydrological rainfall-runoff model. Fig. 17 shows the daily forecasted inflow to Bukan reservoir by the runoff forecast system and observed inflow to Bukan reservoir in 2020 and 2021. We note that the runoff forecasting model generates accurate forecasts in both dry and wet months, with an overall NSE value of 0.66 for two consecutive years. Forecast performance is better in wet months. This time period is important because there is a possibility of floods at this time and because it is a non-agricultural season during which optimal management of the reservoir could maximize surplus water allocations for meeting the environmental needs of UL. The model was also able to forecast days of peak inflow on March 18th and April 8th 2020, and March 15th 2021; forecasting these days is essential from two perspectives. First, it can lead to better flood management and thereby reduce downstream damages. Second, forecasting the volume of water inflow to the reservoir can help in the optimal cultivation planning so that in case of drought, financial losses will not be inflicted on farmers.

**Table 12**
Calibrated parameter values corresponding NSE values for the calibration period.

| Sub-basin | Parameter | Maximum $NSE_Q$ | Maximum $NSE_{LogQ}$ | Minimum Euclidean distance |
|---|---|---|---|---|
| **Saruq river** | SWC [mm] | 354.1 | 219.4 | 310.8 |
| | RRF | 17.5 | 8.9 | 17 |
| | K [mm/day] | 5 | 5 | 5 |
| | $Z_1$ | 20.5 | 8.6 | 16.3 |
| | $T_F$ [°C] | 2.5 | 0.5 | 2.5 |
| | $T_M$ [°C] | 10 | 7.7 | 10 |
| **Khoorkhooreh river** | SWC [mm] | 606.9 | 450.5 | 504.4 |
| | RRF | 5.1 | 2.8 | 5.7 |
| | K [mm/day] | 5 | 5 | 5 |
| | $Z_1$ | 14 | 8.4 | 10.1 |
| | $T_F$ [°C] | 2.2 | 2.4 | 2.1 |
| | $T_M$ [°C] | 3.8 | 3.6 | 3.4 |
| **ZRR upstream** | SWC [mm] | 1234.1 | 195.2 | 242.5 |
| | RRF | 20 | 16.1 | 20 |
| | K [mm/day] | 300 | 6 | 12.5 |
| | $Z_1$ | 5 | 5 | 7.6 |
| | $T_F$ [°C] | 2.5 | 2.5 | 2.5 |
| | $T_M$ [°C] | 10 | 9.4 | 10 |
| **Saqqez river** | SWC [mm] | 1006.9 | 180.3 | 224.5 |
| | RRF | 15.9 | 19.3 | 5.5 |
| | K [mm/day] | 300 | 5 | 12.8 |
| | $Z_1$ | 5.6 | 21.1 | 18.7 |
| | $T_F$ [°C] | 2.5 | 2.5 | 2.5 |
| | $T_M$ [°C] | 10 | 9.9 | 10 |

**Table 13**
NSE values for calibration and validation periods.

| | Calibration period | | Validation period | |
|---|---|---|---|---|
| **Sub-basin** | **$NSE_Q$** | **$NSE_{LogQ}$** | **$NSE_Q$** | **$NSE_{LogQ}$** |
| Saruq river | 0.55 | 0.54 | 0.60 | 0.46 |
| Khoorkhooreh | 0.45 | 0.71 | 0.64 | 0.78 |
| ZRR upstream | 0.33 | 0.64 | 0.50 | 0.51 |
| Saqez river | 0.38 | 0.64 | 0.43 | 0.54 |
| **Average** | **0.43** | **0.63** | **0.54** | **0.57** |

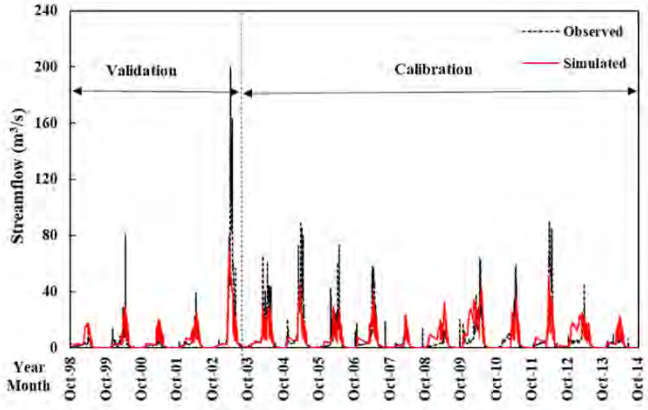


**Fig. 16.** Daily time series of observed and simulated stream flow of Saruq river hydrometric station.

## 5. Conclusion

This study developed and applied the first runoff forecast system on a daily time scale for upstream inflow into Bukan reservoir, a key component of the water management infrastructure in ULB. The forecast system consists of two models: (1) a weather forecast model that downscales the large-scale weather outputs of ECMWF and NCEP to small-scale spatial resolutions and (2) a hydrological rainfall-runoff model that forecasts inflow into Bukan reservoir. The weather forecast downscaling model was developed based on two probabilistic and deterministic approaches and produced temperature and precipitation inputs for the hydrological rainfall-runoff

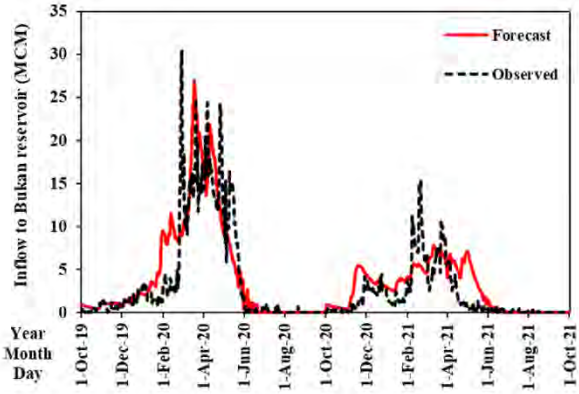


**Fig. 17.** Daily time series of observed and forecasted inflow to Bukan reservoir. The forecasts are made at start of each month with a 1-month lead time.

model. Three deterministic AI methods, including GMDH, SVR, and a hybrid GMDH-SVR method, as well as a probabilistic BBN, were used to downscale the raw precipitation forecasts, while GMDH was used to downscale the raw temperature forecasts. The hydrological rainfall-runoff model includes two storages: (1) snow storage that simulates daily snow accumulation and snowmelt, and (2) soil moisture storage that simulates daily water balance components in the root zone. Calibration of the hydrological model was performed using the MOPSO multi-objective optimization algorithm to estimate hydrological model parameters for each sub-basin upstream of Bukan reservoir. There is no aquifer in the study area.

The weather forecast downscaling model results show that the hybrid method performs much better than the non-hybrid methods for downscaling precipitation. Moreover, ECMWF's precipitation forecast data are more accurate than NCEP for this region. The average NSE of the hybrid method for ECMWF's 1-month lead time forecast downscaled to individual rain gauges was 0.53 and 0.62 for train and test data, respectively. By comparing the forecast precipitation of BBN and the hybrid AI method, BBN has better performance due to its probabilistic feature that helps forecast precipitation with high uncertainty. For instance, the NSE of BBN and hybrid AI for forecasting monthly precipitation were 0.88 and 0.61, respectively, in 2020 and 2021. Temperature forecast data of both organizations, ECMWF and NCEP, had acceptable accuracy and similar performance. The average NSE for train and test data, respectively, were 0.79 and 0.85 for ECMWF and 0.85 and 0.83 for NCEP forecasts with a 6-month lead time.

The calibration of the hydrological rainfall-runoff model indicates that there is no significant trade-off between maximizing objective functions for low and high flows, and improving one objective function does not deteriorate the performance of the other one. In addition, the results show that two-objective calibration reduces the uncertainty in estimating the calibration parameters compared to single-objective calibration. The average NSE in the calibration period was 0.43 and 0.63, and in the validation period, 0.54 and 0.55, respectively, for flow and logarithm of flow. Furthermore, the runoff forecast system resulted in daily forecasts of inflow into Bukan reservoir with an NSE of 0.67 in 2020 and 2021.

We conclude that the runoff forecast system developed in this study has high accuracy in forecasting inflow into Bukan reservoir. Policymakers and operators of the reservoir can use the system to forecast inflows to Bukan reservoir and optimize water allocation between agricultural and environmental demands. Moreover, this system could be beneficial to trigger prior managerial planning and actions before severe droughts or floods happen. The system used in this research can be implemented on other sub-basins and reservoirs in ULB to aid runoff forecasting and optimal management of water resources.

## CRediT authorship contribution statement

**Amirreza Meydani:** Conceptualization, Methodology, Software, Data Curation, Visualization, Writing - Original draft, **Amirhossein Dehghanipour:** Conceptualization, Methodology, Software, Formal Analysis, Writing - Review and Editing, **Gerrit Schoups:** Conceptualization, Methodology, Validation, Investigation, Writing - Review and Editing, **Masoud Tajrishy:** Resources, Writing - Review and Editing, Investigation, Supervision.

## Declaration of Competing Interest

The authors declare that they have no known competing financial interests or personal relationships that could have appeared to influence the work reported in this paper.

## Data availability

Data will be made available on request.

## Appendix A. Supporting information

Supplementary data associated with this article can be found in the online version at doi:10.1016/j.ejrh.2022.101228.

## References


[dataset] ECMWF, 2021a. Seasonal forecast monthly statistics on single levels [WWW Document]. https://doi.org/10.24381/cds.68dd14c3.

[dataset] ECMWF, 2021b. Seasonal forecast daily and subdaily data on single levels [WWW Document]. https://doi.org/10.24381/cds.181d637e.

[dataset] NCEP, 2011. CFSv2 Operational Forecasts Time Series [WWW Document]. URL ⟨https://www.ncei.noaa.gov/products/weather-climate-models/climate-forecast-system⟩.

Adamowski, J., 2013. Using support vector regression to predict direct runoff, base flow and total flow in a mountainous watershed with limited data in Uttaranchal, India. Ann. Warsaw Univ. Life Sci. - SGGW. L. Reclam. 45, 71–83. https://doi.org/10.2478/sggw-2013–0007.

Ahmadaali, J., Barani, G.-A., Qaderi, K., Hessari, B., 2017. Calibration and validation of model WEAP21 for Zarrineh Rud and Simineh Rud basins. Iran. J. Soil Water Res. 48, 823–839. https://doi.org/10.22059/ijswr.2017.216989.667543.

Ahmadi, A., Nasseri, M., Solomatine, D.P., 2019. Parametric uncertainty assessment of hydrological models: coupling UNEEC-P and a fuzzy general regression neural network. Hydrol. Sci. J. 64, 1080–1094. https://doi.org/10.1080/02626667.2019.1610565.

Arpe, K., Leroy, S.A.G., Wetterhall, F., Khan, V., Hagemann, S., Lahijani, H., 2014. Prediction of the Caspian Sea level using ECMWF seasonal forecasts and reanalysis. Theor. Appl. Climatol. 117, 41–60. https://doi.org/10.1007/s00704-013-0937-6.

BayesFusion, L. L. C. (2017). GeNIe Modeler. *User Manual. Available online: https://support.bayesfusion.com/docs/(accessed on 21 October 2019)*.

Benderskaya, E.N., 2013. Nonlinear Trends in Modern Artificial Intelligence: A New Perspective. In: Kelemen, J., Romportl, J., Zackova, E. (Eds.), Beyond Artificial Intelligence. Topics in Intelligent Engineering and Informatics, 4. Springer, Berlin, Heidelberg. 10.1007/978-3-642-34422-0_8.

Chen, Y., Sharma, S., Zhou, X., Yang, K., Li, X., Niu, X., Hu, X., Khadka, N., 2021. Spatial performance of multiple reanalysis precipitation datasets on the southern slope of central Himalaya. Atmos. Res. 250, 105365 https://doi.org/10.1016/j.atmosres.2020.105365.

Chevalier, R.F., Hoogenboom, G., McClendon, R.W., Paz, J.A., 2011. Support vector regression with reduced training sets for air temperature prediction: a comparison with artificial neural networks. Neural Comput. Appl. 20, 151–159. https://doi.org/10.1007/s00521-010-0363-y.

Coello, C.A.C., Pulido, G.T., Lechuga, M.S., 2004. Handling multiple objectives with particle swarm optimization. IEEE Trans. Evol. Comput. 8, 256–279. https://doi.org/10.1002/9780470612163.

Dariane, A.B., Pouryafar, E., 2021. Quantifying and projection of the relative impacts of climate change and direct human activities on streamflow fluctuations. Clim. Change 165, 34. https://doi.org/10.1007/s10584-021-03060-w.

Dehghanipour, A.H., Zahabiyoun, B., Schoups, G., Babazadeh, H., 2019. A WEAP-MODFLOW surface water-groundwater model for the irrigated Miyandoab plain, Urmia lake basin, Iran: multi-objective calibration and quantification of historical drought impacts. Agric. Water Manag. 223, 105704 https://doi.org/10.1016/j.agwat.2019.105704.

Dehghanipour, A.H., Schoups, G., Zahabiyoun, B., Babazadeh, H., 2020. Meeting agricultural and environmental water demand in endorheic irrigated river basins: a simulation-optimization approach applied to the Urmia Lake basin in Iran. Agric. Water Manag. 241, 106353 https://doi.org/10.1016/j.agwat.2020.106353.

Dehghanipour, M.H., Karami, H., Ghazvinian, H., Kalantari, Z., Dehghanipour, A.H., 2021. Two comprehensive and practical methods for simulating pan evaporation under different climatic conditions in Iran. Water 13, 2814. https://doi.org/10.3390/w13202814.

Dodangeh, E., Panahi, M., Rezaie, F., Lee, S., Tien, D., 2020. Novel hybrid intelligence models for flood-susceptibility prediction: meta optimization of the GMDH and SVR models with the genetic algorithm and harmony search. J. Hydrol. 590, 125423 https://doi.org/10.1016/j.jhydrol.2020.125423.

Dunn, S.M., Stalham, M., Chalmers, N., Crabtree, B., 2003. Adjusting irrigation abstraction to minimise the impact on stream flow in the east of Scotland. J. Environ. Manag. 68, 95–107. https://doi.org/10.1016/S0301-4797(03)00006-9.

ECMWF, 2013. IFS documentation – Cy38r1, Part III: Dynamics and numerical procedures Table of contents. Shinfield Park, Reading, RG2 9AX, England.

Emami, F., Koch, M., 2019. Modeling the impact of climate change on water availability in the Zarrine River basin and inflow to the Boukan Dam, Iran. Climate 7. https://doi.org/10.3390/cli7040051.

Fawcett, T., 2006. An introduction to ROC analysis. Pattern Recognit. Lett. 27, 861–874. https://doi.org/10.1016/j.patrec.2005.10.010.

Ficchì, A., Raso, L., Dorchies, D., Pianosi, F., Malaterre, P.-O., Van Overloop, P.-J., Jay-Allemand, M., 2016. Optimal operation of the multireservoir system in the Seine River basin using deterministic and ensemble forecasts. J. Water Resour. Plan. Manag. 142, 05015005 (10.1061/(asce)wr.1943-5452.0000571).

Gavahi, K., Mousavi, S.J., Ponnambalam, K., 2019. Adaptive forecast-based real-time optimal reservoir operations: application to Lake Urmia. J. Hydroinformatics 21, 908–924. https://doi.org/10.2166/hydro.2019.005.

Geng, J., Gan, W., Xu, J., Yang, R., Wang, S., 2020. Support vector machine regression (SVR)-based nonlinear modeling of radiometric transforming relation for the coarse-resolution data-referenced relative radiometric normalization (RRN). Geo-Spat. Inf. Sci. 23, 237–247. https://doi.org/10.1080/10095020.2020.1785958.

Ghaheri, M., Baghal-Vayjooee, M.H., Naziri, J., 1999. Lake Urmia, Iran: a summary review. Int. J. Salt Lake Res. 8, 19–22. https://doi.org/10.1007/bf02442134.

Goodarzi, L., Banihabib, M.E., Roozbahani, A., Dietrich, J., 2019. Bayesian network model for flood forecasting based on atmospheric ensemble forecasts. Nat. Hazards Earth Syst. Sci. 19, 2513–2524. https://doi.org/10.5194/nhess-19-2513-2019.

Govender, I.H., Sahlin, U., O'Brien, G.C., 2021. Bayesian network applications for sustainable holistic water resources management: modeling opportunities for South Africa. Risk Anal. 0, risa.13798 https://doi.org/10.1111/risa.13798.

Grillakis, M., Koutroulis, A., Tsanis, I., 2018. Improving seasonal forecasts for basin scale hydrological applications. Water 10, 1593. https://doi.org/10.3390/w10111593.

Gubler, S., Sedlmeier, K., Bhend, J., Avalos, G., Coelho, C.A.S., Escajadillo, Y., Jacques-Coper, M., Martinez, R., Schwierz, C., de Skansi, M., Spirig, C., 2020. Assessment of ECMWF SEAS5 seasonal forecast performance over South America. Weather Forecast 35, 561–584. https://doi.org/10.1175/WAF-D-19-0106.1.

Her, Y., Seong, C., 2018. Responses of hydrological model equifinality, uncertainty, and performance to multi-objective parameter calibration. J. Hydroinformatics 20, 864–885. https://doi.org/10.2166/hydro.2018.108.

Hrachowitz, M., Clark, M.P., 2017. HESS Opinions: The complementary merits of competing modelling philosophies in hydrology 3953–3973.

Hruschka, E.R., Nicoletti, M., do, C., 2013. Roles played by Bayesian networks in machine learning: an empirical investigation. Smart Innov. Syst. Technol. 13, 75–116. https://doi.org/10.1007/978-3-642-28699-5_5.

Ivakhnenko, A.G., 1970. Heuristic self-organization in problems of engineering cybernetics. Automatica 6, 207–219. https://doi.org/10.1016/0005-1098(70)90092-0.

Johnson, S.J., Stockdale, T.N., Ferranti, L., Balmaseda, M.A., Molteni, F., Magnusson, L., Tietsche, S., Decremer, D., Weisheimer, A., Balsamo, G., Keeley, S.P.E., Mogensen, K., Zuo, H., Monge-sanz, B.M., Park, S., 2019. SEAS5: the new ECMWF seasonal forecast system 1087–1117.

Kaune, A., Chowdhury, F., Werner, M., Bennett, J., 2020. The benefit of using an ensemble of seasonal streamflow forecasts in water allocation decisions. Hydrol. Earth Syst. Sci. 24, 3851–3870. https://doi.org/10.5194/hess-24-3851-2020.

Khan, M.S., Coulibaly, P., 2006. Bayesian neural network for rainfall-runoff modeling. Water Resour. Res. 42, 1–18. https://doi.org/10.1029/2005WR003971.

Khorasani, H., Kerachian, R., Malakpour-Estalaki, S., 2018. Developing a comprehensive framework for eutrophication management in off-stream artificial lakes. Journal of Hydrology 562, 103–124. https://doi.org/10.1016/j.jhydrol.2018.04.052.

Kisi, O., Cimen, M., 2012. Precipitation forecasting by using wavelet-support vector machine conjunction model. Eng. Appl. Artif. Intell. 25, 783–792. https://doi.org/10.1016/j.engappai.2011.11.003.

Lang, Y., Luo, L., Ye, A., Duan, Q., 2020. Do CFSv2 seasonal forecasts help improve the forecast of meteorological drought 1–14. ⟨https://doi.org/10.3390/w12072010⟩.
Liu, Y., Wang, H., Lei, X., Wang, H., 2021. Real-time forecasting of river water level in urban based on radar rainfall: a case study in Fuzhou City. J. Hydrol. 603, 126820 https://doi.org/10.1016/j.jhydrol.2021.126820.
Mahmudi, P., Motamedvaziri, B., Hosseini, M., Ahmadi, H., Amini, A., 2021. Study of climate change effects on hydrological processes in Siminehroud and Zarrinehroud watersheds northwest of Iran Study of climate change effects on hydrological processes in Siminehroud and Zarrinehroud watersheds northwest of Iran. ⟨https://doi.org/10.1007/s12145–021-00598–2⟩.
Mancosu, N., Snyder, R.L., Kyriakakis, G., Spano, D., 2015. Water scarcity and future challenges for food production. Water 7, 975–992. https://doi.org/10.3390/w7030975.
Meydani, A., Dehghanipour, A., Tajrishy, M., 2021. Development of a daily rainfall-runoff model to simulate the Bukan reservoir inflow and quantify the effects of severe historical drought using WEAP model and multiobjective calibration. Iran. -Water Resour. Res. 17, 149–164.
Molina, J.L., Pulido-Velázquez, D., García-Aróstegui, J.L., Pulido-Velázquez, M., 2013. Dynamic Bayesian networks as a decision support tool for assessing climate change impacts on highly stressed groundwater systems. J. Hydrol. 479, 113–129. https://doi.org/10.1016/j.jhydrol.2012.11.038.
Moriasi, D.N., Arnold, J.G., Liew, M.W., Van, Bingner, R.L., Harmel, R.D., Veith, T.L., 2007. Model evaluation guidlines for systematic quantification of accuracy in watershed simulations. Trans. ASABE 50, 885–900.
Mostafazade, M., Alizadeh, H., 2020. Calibration of a water resource planning model using many-objective optimization. Iran. -Water Resour. Res. 15, 200–213.
Munoz, P., Munoz, D.F., Orellana-Alvear, J., Moftakhari, H., Moradkhani, H., Celleri, R., 2021. Long short-term memory networks for real-time runoff forecasting using remotely sensed data, in: EGU General Assembly. pp. 19–30. ⟨https://doi.org/10.5194/egusphere-egu21–13900⟩, 2021.
Nariman-zadeh, N., Darvizeh, A., Darvizeh, M., Gharababaei, H., 2002. Modelling of explosive cutting process of plates using GMDH-type neural network and singular value decompositio. J. Mater. Process. Technol 128, 80–87. https://doi.org/10.1016/S0924-0136(02)00264-9.
Oudin, L., Andréassian, V., Mathevet, T., Perrin, C., Michel, C., 2006. Dynamic averaging of rainfall-runoff model simulations from complementary model parameterizations. Water Resour. Res. 42, 1–10. https://doi.org/10.1029/2005WR004636.
Owens, R., Hewson, T., 2018. ECMWF Forecast User Guide. https://doi.org/10.21957/m1cs7h.
Phan, T.D., Smart, J.C.R., Capon, S.J., Hadwen, W.L., Sahin, O., 2016. Applications of Bayesian belief networks in water resource management: a systematic review. Environ. Model. Softw. 85, 98–111. https://doi.org/10.1016/j.envsoft.2016.08.006.
Phan-Van, T., Nguyen-Xuan, T., Van Nguyen, H., Laux, P., Pham-Thanh, H., Ngo-Duc, T., 2018. Evaluation of the NCEP climate forecast system and its downscaling for seasonal rainfall prediction over Vietnam. Weather Forecast 33, 615–640. https://doi.org/10.1175/WAF-D-17-0098.1.
Pushpalatha, R., Perrin, C., Le, N., Andréassian, V., 2012. A review of efficiency criteria suitable for evaluating low-flow simulations. J. Hydrol. 420–421, 171–182. https://doi.org/10.1016/j.jhydrol.2011.11.055.
Rayner, S., Lach, D., Ingram, H., 2005. Weather forecasts are for wimps: why water resource managers do not use climate forecasts. Clim. Change 69, 197–227. https://doi.org/10.1007/s10584-005-3148-z.
Roodari, A., Hrachowitz, M., Hassanpour, F., Yaghoobzadeh, M., 2020. Signatures of human intervention – or not? Downstream intensification of hydrological drought along a large Central Asian River: the individual roles of climate variability and land use change. Hydrol. Earth Syst. Sci. Discuss. 1–40. https://doi.org/10.5194/hess-2020-369.
Saha, S., Moorthi, S., Pan, H.L., Wu, X., Wang, Jiande, Nadiga, S., Tripp, P., Kistler, R., Woollen, J., Behringer, D., Liu, H., Stokes, D., Grumbine, R., Gayno, G., Wang, Jun, Hou, Y.T., Chuang, H.Y., Juang, H.M.H., Sela, J., Iredell, M., Treadon, R., Kleist, D., Van Delst, P., Keyser, D., Derber, J., Ek, M., Meng, J., Wei, H., Yang, R., Lord, S., Van Den Dool, H., Kumar, A., Wang, W., Long, C., Chelliah, M., Xue, Y., Huang, B., Schemm, J.K., Ebisuzaki, W., Lin, R., Xie, P., Chen, M., Zhou, S., Higgins, W., Zou, C.Z., Liu, Q., Chen, Y., Han, Y., Cucurull, L., Reynolds, R.W., Rutledge, G., Goldberg, M., 2010. The NCEP climate forecast system reanalysis. Bull. Am. Meteorol. Soc. 91, 1015–1057. https://doi.org/10.1175/2010BAMS3001.1.
Saha, S., Moorthi, S., Wu, X., Wang, J., Nadiga, S., Tripp, P., Behringer, D., Hou, Y.T., Chuang, H.Y., Iredell, M., Ek, M., Meng, J., Yang, R., Mendez, M.P., Van Den Dool, H., Zhang, Q., Wang, W., Chen, M., Becker, E., 2014. The NCEP climate forecast system version 2. J. Clim. 27, 2185–2208. https://doi.org/10.1175/JCLI-D-12-00823.1.
Sangelantoni, L., Ferretti, R., Redaelli, G., 2019. Toward a regional-scale seasonal climate prediction system over central Italy based on dynamical downscaling. Climate 7. https://doi.org/10.3390/cli7100120.
Schoups, G., Addams, C.L., Gorelick, S.M., 2005. Multi-objective calibration of a surface water-groundwater flow model in an irrigated agricultural region: Yaqui Valley, Sonora, Mexico. Hydrol. Earth Syst. Sci. 9, 549–568. https://doi.org/10.5194/hess-9-549-2005.
Siegmund, J., Bliefernicht, J., Laux, P., Kunstmann, H., 2015. Toward a seasonal precipitation prediction system for West Africa: performance of CFSv2 and high-resolution dynamical downscaling. J. Geophys. Res. 120, 7316–7339. https://doi.org/10.1002/2014JD022692.
Sisto, N.P., 2009. Environmental flows for rivers and economic compensation for irrigators. J. Environ. Manag. 90, 1236–1240. https://doi.org/10.1016/j.jenvman.2008.06.005.
Sodoudi, S., Noorian, A., Geb, M., Reimer, E., 2010. Daily precipitation forecast of ECMWF verified over Iran. Theor. Appl. Climatol. 99, 39–51. https://doi.org/10.1007/s00704-009-0118-9.
Sun, L., Lan, Y., 2021. Statistical downscaling of daily temperature and precipitation over China using deep learning neural models: localization and comparison with other methods. Int. J. Climatol. 41, 1128–1147. https://doi.org/10.1002/joc.6769.
Sun, S., Leonhardt, G., Sandoval, S., Bertrand-Krajewski, J.L., Rauch, W., 2017. A Bayesian method for missing rainfall estimation using a conceptual rainfall–runoff model. Hydrol. Sci. J. 62, 2456–2468. https://doi.org/10.1080/02626667.2017.1390317.
Valipour, M., Ziatabar Ahmadi, M., Raeini-Sarjaz, M., Gholami Sefidkouhi, M.A., Shahnazari, A., Fazlola, R., Darzi-Naftchali, A., 2015. Agricultural water management in the world during past half century. Arch. Agron. Soil Sci. 61, 657–678. https://doi.org/10.1080/03650340.2014.944903.
Valverde Ramírez, M.C., Ferreira, N.J., de Campos Velho, H.F., 2006. Linear and nonlinear statistical downscaling for rainfall forecasting over southeastern Brazil. Weather Forecast 21, 969–989. https://doi.org/10.1175/WAF981.1.
Voisin, N., Pappenberger, F., Lettenmaier, D.P., Buizza, R., Schaake, J.C., 2011. Application of a medium-range global hydrologic probabilistic forecast scheme to the Ohio River basin. Weather Forecast 26, 425–446. https://doi.org/10.1175/WAF-D-10-05032.1.
Wang, F., Wang, L., Zhou, H., Valeriano, O.C.S., Koike, T., Li, W., 2012. Ensemble hydrological prediction-based real-time optimization of a multiobjective reservoir during flood season in a semiarid basin with global numerical weather predictions. Water Resour. Res. 48, 1–21. https://doi.org/10.1029/2011WR011366.
Xue, J., Gui, D., Lei, J., Sun, H., Zeng, F., Feng, X., 2017. A hybrid Bayesian network approach for trade-offs between environmental flows and agricultural water using dynamic discretization. Adv. Water Resour. 110, 445–458. https://doi.org/10.1016/j.advwatres.2016.10.022.
Yaghoubi, B., Hosseini, S.A., Nazif, S., 2019. Monthly prediction of streamflow using data-driven models. J. Earth. Syst. Sci. 128, 141 https://doi.org/10.1007/s12040-019-1170-1.
Yates, D., Sieber, J., Purkey, D., Huber-Lee, A., 2005. WEAP21 – a demand-, priority-, and preference-driven water planning model: part 1: model characteristics. Water Int. 30, 487–500. https://doi.org/10.1080/02508060508691893.
Yekom Consulting Engineers, 2016. Implementing solutions to reduce the agricultural water consumption of the Zarrinehrood and Siminehrood sub-basin by 40% (In Persian).
Yuan, X., Wood, E.F., Roundy, J.K., Pan, M., 2013. CFSv2-based seasonal hydroclimatic forecasts over the conterminous United States. J. Clim. 26, 4828–4847. https://doi.org/10.1175/JCLI-D-12-00683.1.